SCIENTIFIC REP♀RTS

OPEN

Aspermerodione, a novel fungal metabolite with an unusual 2,6-dioxabicyclo[2.2.1]heptane skeleton, as an inhibitor of penicillin-binding protein 2a

Yuben Qiao[1], Xiaotian Zhang[1,2], Yan He[1,3], Weiguang Sun[1], Wenya Feng[1], Junjun Liu[1], Zhengxi Hu[1], Qianqian Xu[1], Hucheng Zhu[1], Jinwen Zhang[2], Zengwei Luo[1], Jianping Wang[1], Yongbo Xue[1] & Yonghui Zhang[1]

Rising drug resistance limits the treatment options infected by methicillin-resistant *Staphylococcus aureus* (MRSA). A promising solution for overcoming the resistance of MRSA is to inhibit the penicillin-binding protein 2a (PBP2a). A novel terpene-polyketide hybrid meroterpenoid, aspermerodione (1), characterized by an unusual 2,6-dioxabicyclo[2.2.1]heptane core skeleton, and a new heptacyclic analogue, andiconin C (2), were isolated and identified from the liquid cultures of endophytic fungus *Aspergillus* sp. TJ23. The structures and their absolute configurations of all chiral centers were elucidated via extensive spectroscopic analyses and electronic circular dichroism (ECD) calculations and determined via single-crystal X-ray diffraction analysis. Aspemerodione (1) was found to be a potential inhibitor of PBP2a, and work synergistically with the β-lactam antibiotics oxacillin and piperacillin against MRSA.

Methicillin-resistant *Staphylococcus aureus* (MRSA) is one of the most prevalent multidrug-resistant pathogens worldwide, and it represents a major public health problem[1]. Over the past several decades, the emergence of methicillin-resistant MRSA and its rapid spread has led to the increasing difficulty in treating MRSA infection[2,3]. MRSA acquires a series of drug-resistance gene mutations, as exemplified by *mec*A, and encodes penicillin-binding protein 2a (PBP2a), which is resistant to most β-lactam antibiotics[4]. PBP2a specifically plays vital role on crosslinking of the cell wall, even when other PBPs are inhibited by β-lactam antibiotics[5,6]. The underlying mechanism is involved in allostery mediated inactivated conformation for the active site[7,8].

Recent studies have demonstrated that the combined use of small molecules that bind to the allosteric active site of PBP2a can render MRSA sensitive to the effects of conventional β-lactam antibiotics[9,10]. To this end, the inhibition of PBP2a is a hopeful solution for overcoming the multiple drug resistance of MRSA via preserving the availability of therapeutic agents that are already useful in the pharmacological armamentarium[9].

In our efforts to identify novel and bioactive compounds from Chinese traditional medicins (TCMs) and their endophytic microbial sources[11–13], an extensive biological screen against MRSA (ATCC43300) *in vitro* was conducted, and the endophytic fungus *Aspergillus* sp. TJ23 showed the best bioactivity against the indicator bacteria. Spiroaspertrione A, a metabolite of *Aspergillus* sp. TJ23 that has a novel terpene–polyketide skeleton, shows potent resensitisation of oxacillin against MRSA[13]. Since the secondary metabolites was significantly effected by

[1]Hubei Key Laboratory of Natural Medicinal Chemistry and Resource Evaluation, School of Pharmacy, Tongji Medical College, Huazhong University of Science and Technology, Wuhan, 430030, Hubei Province, People's Republic of China. [2]Biological Engineering, Wuchang Shouyi University, Wuhan, 430064, China. [3]Tongji Hospital Affiliated to Tongji Medical College, Huazhong University of Science and Technology, Wuhan, 430030, People's Republic of China. Yuben Qiao, Xiaotian Zhang, Yan He and Weiguang Sun contributed equally to this work. Correspondence and requests for materials should be addressed to J.W. (email: 290987243@qq.com) or Y.X. (email: yongboxue@mail.hust.edu.cn) or Y.Z. (email: zhangyh@mails.tjmu.edu.cn)
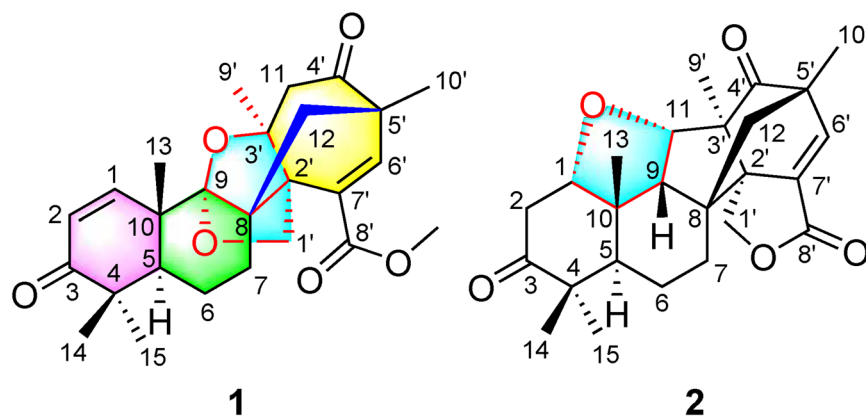
Figure 1. Structures of compounds **1** and **2**.

the culture medium[14], we preliminarily investigated the influence on the secondary productions of the endophytic fungus *Aspergillus* sp. TJ23 in a liquid broth.

Isolation of the liquid cultures of this fungal strain yielded two polycyclic terpene–polyketide hybrid meroterpenoids (Fig. 1), aspermerodione (**1**), which is characterized by the incorporation of a rare 2,6-dioxabicyclo[2.2.1] heptane group into the spiro[bicyclo[3.2.2]nonane-2,1′-cyclohexane] ring system, and a new heptacyclic analogue, andiconin C (**2**). Herein, the isolation, structural elucidation, plausible biosynthetic pathway, and bioactivities of compounds **1** and **2** are presented.

Results and Discussion

Structural elucidation of the isolates. Compound **1** was isolated as colorless crystals (in $CHCl_3$–MeOH). The molecular formula of **1** was determined to be $C_{26}H_{32}O_6$ by the positive ion peaks at m/z 441.2251 $[M+H]^+$ and 463.2049 $[M+Na]^+$ in the HRESIMS spectrum, denoting 11 degrees of unsaturation. The ^1H NMR spectrum (Table 1) of **1** demonstrated six sp³ singlet methyls at δ_H 1.07 (H_3-14), 1.12 (H_3-15), 1.21 (H_3-13), 1.29 (H_3-10′), 1.45 (H_3-9′), and 3.73 (OCH₃-8′), and three olefinic protons at δ_H 7.27 (d, $J=10.0$, H-1), 5.87 (d, $J=10.0$, H-2), and 6.87 (s, H-6′). Additionally, the ^{13}C NMR and DEPT spectra (Table 1) revealed 26 carbon atom resonances corresponding to six sp³ methyls (including one oxygenated), five methylenes (including one oxygenated), one sp³ methine at δ_C 46.5 (C-5), and seven sp³ quaternary carbons [including one ketal carbon at δ_C 109.3 (C-9)]. Three carbonyl groups and four olefinic carbon atoms, accounting for 5 out of 11 degrees of unsaturation, indicated that **1** possessed a hexacyclic ring system.

All proton resonances were assigned to their respective carbons with the help of HSQC spectrum. Comparison of the HRESIMS and spectroscopic data of **1** with previously reported meroterpenoids[15], prompted us to consider that compound **1** was an unusual rearranged meroterpenoid comprising two subunits, A and B, which were subsequently ascertained as follows (Fig. 2 and Fig. S19, Supplementary Information). The key HMBC correlations from H-1, H_3-14, and H_3-15 to C-3 and C-5; from H-2, H_3-14, and H_3-15 to C-4; from H-5 to C-7, C-10, and C-13; and from H_3-13 to C-1, C-5, C-9, and C-10, combined with the spin-spin coupling systems of H-1/H-2 and H-5/H_2-6/H_2-7 in its ^1H–^1H COSY spectrum, indicated the presence of subunit A. In addition, the subunit B was constructed by the key HMBC correlations from H_3-9′ to C-2′, C-3′, and C-11; from H_3-10′ to C-4′, C-6′, and C-12; from H-6′ to C-2′, C-4′, C-8′, and C-10′; from H_2-12 to C-4′ and C-6′, and from OCH₃-8′ to C-8′. The fusion of subunits A and B was deduced based on the obvious HMBC (Fig. 2) correlations from H_2-12 and H_2-1′ to C-8 and C-9, which displayed the direct carbon-carbon connectivity of C-12 and C-8 and ether bridge linkage between C-1′ and C-9. Given the index of hydrogen deficiency of 11 from its molecular formula, the carbon resonance of C-9 (δ_C 109.3) in **1** was observed to significantly shift downfield, to which we assigned the existence of another O-linkage at C-9/C-3′ to generate an unusual 2,6-dioxabicyclo[2.2.1]heptane core scaffold. Thus, the planar structure of **1** was established as shown in Fig. 1.

Based on a detailed analysis of the NOESY (Fig. 3) spectrum of **1** and referring the bio-origin of paralleled meroterpenoids[13,15], the relative configuration of **1** was established. Structurally, the relative configuration of H-5 of paralleled meroterpenoids was α-oriented[15,16]. The obvious NOESY correlations (Fig. 3) of H-5/H_3-15, H-5/H_2-7, H_2-7/H_2-1′, and of H_2-1′/H_3-9′, indicated that these protons are all on the same side of molecule and assigned as the α-orientation. In contrast, the key NOESY correlations from H_3-13 to H_3-14 and H_2-12 displayed in its NOESY spectrum (Fig. 3), showed they are on the opposite face on the molecule and assigned to the β-orientation. The relative configuration of **1** was thus established as 2′R*,3′S*,5S*,5′S*,8R*,9R*,10S*.

To elucidate the absolute configurations of all chiral centers of **1**, a time-dependent density functional theory (TDDFT) method at the B3LYP/6-311++G** level with PCM in MeOH was performed for 2′R,3′S,5S,5′S,8R,9R,10S-**1** (Fig. 4), in which the experimental ECD spectrum of **1** was in good agreement with its calculated ECD curve, indicating that the absolute configuration of **1** was 2′R,3′S,5S,5′S,8R,9R,10S (Fig. 1).

A suitable crystal of **1** was obtained by slow evaporation of a mixture of $CHCl_3$–MeOH (10:1) at room temperature, and subjected to a single-crystal X-ray diffraction experiment using Cu Kα radiation (Fig. 5, CCDC 1554255)[17], which supported the proposed structure and its absolute configuration. It was given the name

| No.	1 (in CDCl$_3$) δ_H J in Hz	δ_C type	2 (in CDCl$_3$) δ_H J in Hz	δ_C type
1	7.27, d (10.0)	155.4, CH	3.62, t (7.1)	84.1, CH
2	5.87, d (10.0)	126.2, CH	2.76, overlap; 2.78, overlap	40.0, CH$_2$
3		204.2, C		214.4, C
4		44.3, C		46.0, C
5	2.33, m	46.5, CH	1.78, m	41.6, CH
6	1.67, m	18.5, CH$_2$	1.60, m; 1.71, m	17.5, CH$_2$
7	1.25, m; 1.62, m	30.9, CH$_2$	1.78, m; 1.93, m	29.3, CH$_2$
8		53.5, C		57.1, C
9		109.3, C	1.96, d (6.6)	65.1, CH
10		41.6, C		45.5, C
11	2.50, d (19.0)	51.2, CH$_2$	3.95, d (6.6)	86.9, CH
	2.65, d (19.0)			
12	1.46, overlap	38.1, CH$_2$	1.56, d (5.2)	59.2, CH$_2$
	2.20, d (14.9)		1.61, d (5.2)	
13	1.21, s	18.9, CH$_3$	0.90, s	20.9, CH$_3$
14	1.07, s	21.2, CH$_3$	1.01, s	18.5, CH$_3$
15	1.12, s	28.3, CH$_3$	1.14, s	28.5, CH$_3$
1′	4.03, d (9.1)	67.2, CH$_2$	4.71, d (10.4)	70.3, CH$_2$
	4.69, d (9.1)		5.93, d (10.4)	
2′		55.8, C		59.7, C
3′		84.1, C		46.1, C
4′		200.6, C		211.2, C
5′		50.8, C		52.2, C
6′	6.87, s	145.3, CH	7.08, s	142.7, CH
7′		130.3, C		134.3, C
8′		164.6, C		166.9, C
9′	1.45, s	27.6, CH$_3$	1.18, s	13.6, CH$_3$
10′	1.29, s	22.3, CH$_3$	1.31, s	16.9, CH$_3$
OCH$_3$-8′	3.73, s	52.0, CH$_3$		

Table 1. ^{1}H NMR (400 MHz) and ^{13}C NMR (100 MHz) spectroscopic data for compounds **1** and **2**.
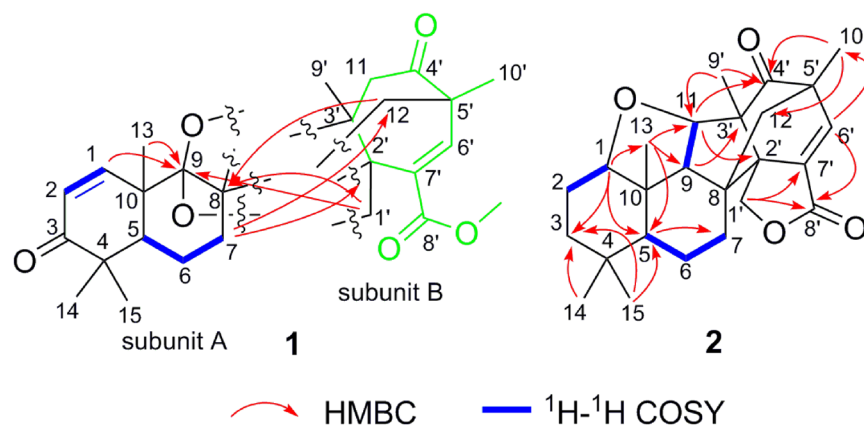

Figure 2. Key HMBC and ^{1}H–^{1}H COSY correlations of compounds **1** and **2**.

aspermerodione, which featured the incorporation of a rare 2,6-dioxabicyclo[2.2.1]heptane moiety into the spiro[bicyclo[3.2.2]nonane-2,1′-cyclohexane] ring system.

Compound **2** was obtained as an optically active, colorless crystal (in CHCl$_3$–MeOH). The HRESIMS analysis of **2** displayed a sodiated ion peak at m/z 433.1961 [M + Na]$^+$ and a protonated ion peak at m/z 411.2146 [M + H]$^+$, and we determined its molecular formula to be C$_{25}$H$_{30}$O$_5$, denoting 11 degrees of unsaturation. The ^{1}H NMR spectrum (Table 1) of **2** showed signals attributed to five singlet methyls at δ_H 0.90 (H$_3$-13), 1.01 (H$_3$-14), 1.14 (H$_3$-15), 1.18 (H$_3$-9′), and 1.31 (H$_3$-10′), one oxygenated sp^3 methylene at δ_H 4.93 and 4.71 (both d,
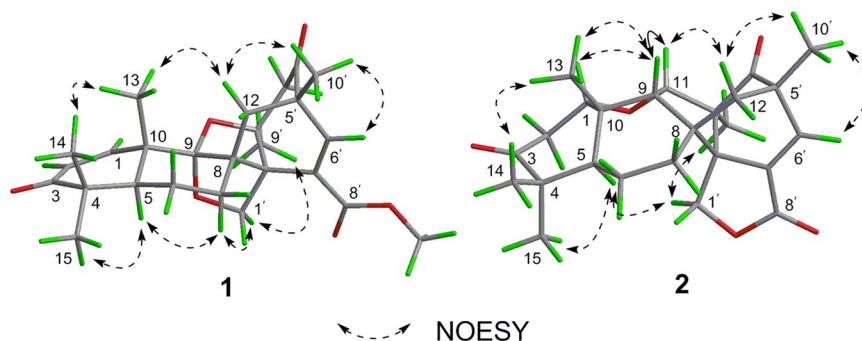
**Figure 3.** Key NOESY correlations of compounds **1** and **2**.
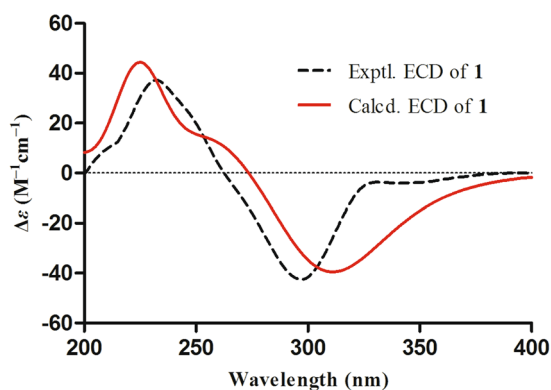
Figure 4. Experimental and calculated ECD spectra of **1** recorded in MeOH.
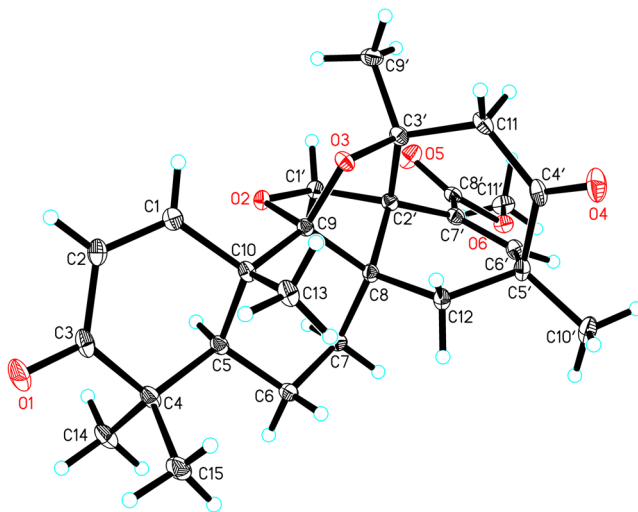

Figure 5. X-ray ORTEP drawing of compound **1**.

$J = 10.4$ Hz, H$_2$-1′), two oxygenated sp^3 methines at δ_H 3.62 (t, $J = 7.1$ Hz, H-1) and δ_H 3.95 (d, $J = 6.5$ Hz, H-11), and one olefinic proton signals at δ_H 7.08 (s, H-6′). The ^{13}C NMR and DEPT spectra of **2** (Table 1), displayed resonances for 25 carbon signals that were resolved into three carbonyl carbons at δ_C 166.9 (C-6′), 211.2 (C-4′), and 214.4 (C-3), five methyl groups at δ_C 13.6 (C-9′), 16.9 (C-10′), 18.5 (C-14), 20.9 (C-13), and 28.5 (C-15), five methylenes including one oxygenated [δ_C 17.5 (C-6), 29.3 (C-7), 40.0 (C-2), 59.2 (C-12), and 70.3 (C-1′)], two olefinic carbon signals at δ_C 142.7 (C-6′) and 134.3 (C-7′), four methines including two oxygenated [δ_C 41.6 (C-5), 65.1 (C-9), 84.1 (C-1), and 86.9 (C-1′)], and six sp^3 quaternary carbon atoms at δ_C 45.5 (C-10), 46.0 (C-4), 46.1 (C-3′), 52.2 (C-5′), 57.1 (C-8), and 59.7 (C-2′). The aforementioned spectroscopic data of **2** showed signals similar to those of the known compound, andiconin B[13], indicating that both share an andiconin-type carbocyclic
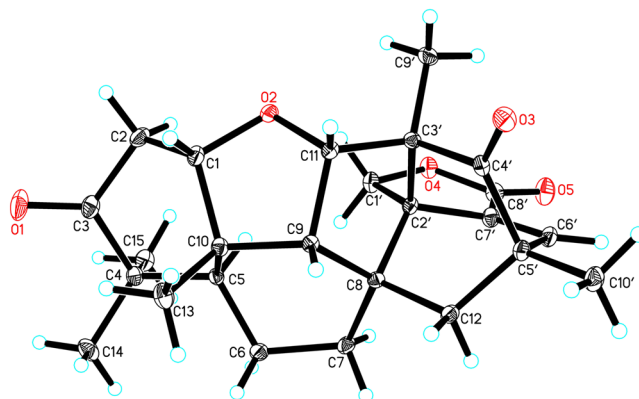
**Figure 6.** X-ray ORTEP drawing of compound **2**.
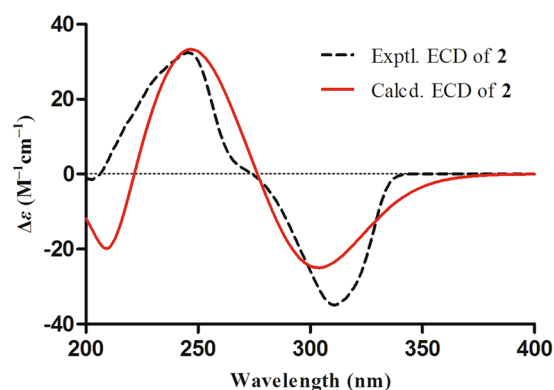
Figure 7. Experimental and calculated ECD spectra of **2** recorded in MeOH.

skeleton, except that a couple of double peak olefinic proton signals (both d, $J = 10.3$ Hz) and a sp³ methine group in andiconin B were replaced by an oxygenated methine and a singlet olefinic proton in **2**. Those variations and one additional degree of unsaturation when compared to andiconin B suggested an oxygen linkage between C-1 and C-11 to form a new ring system and demonstrated the formation of a new double bond with dehydration between C-6′ and C-7′, which was evidenced by the relative downfield shifted carbon resonances of C-6′, C-7′, and C-11, and supported by the significant up-field chemical shifts from 152.6 and 126.5 ppm to 84.1 and 40.0 ppm, respectively, in **2**. This deduction was further verified by the key HMBC (Fig. 2 and Fig. S19, Supplementary Information) correlations from H-1 to C-3, C-5. C-9, C-10, and C-13, and from H-6′ to C-2′, C-4′, C-5′, C-8′, C-10′, and C-12, and further supported by the spin-spin coupling systems of H-1/H$_2$-2 and H-9/H-11 in its ¹H–¹H COSY spectrum (Fig. 2). Thus, the planar structure of **2** was elucidated as shown (Fig. 1).

The relative configuration of **2** was determined by the comprehension of the key NOESY spectrum (Fig. 3) and coupling constants. The obvious NOEs of H-5 with H$_3$-15 and H$_2$-7, H$_2$-7 with H$_2$-1′, and H$_2$-1′ with H$_3$-9′ indicated that those protons were all arbitrarily assigned to the α-orientation. Accordingly, the NOESY correlations of H-1/H$_3$-14/H$_3$-13, H-11/H$_2$-12, and of H-9 with H$_3$-13 and H-11 suggested that they were in the β configuration.

After repeated recrystallization by various solvent systems, **2** furnished a high-quality crystal in a mixture of CHCl$_3$–MeOH (7:3) at room temperature, which was successfully subjected to single-crystal X-ray diffraction using Cu Kα radiation (Fig. 6) with a Flack parameter of –0.03(5) (CCDC 1554256)[17], which enabled us to confirm its absolute configuration as 1S,2′R,3′S,5R,5′S,8S,9R,10S,11S (Fig. 1). To further support this deduction, the calculated ECD spectrum of 1S,2′R,3′S,5R,5′S,8S,9R,10S-**2** was determined at the B3LYP/6–31 G(d,p) level and showed an excellent coincidence with the experimental ECD curve (Fig. 7), which undoubtedly corroborated its absolute structure.

To our knowledge, aspermerodione (**1**) represents a novel meroterpenoid with an unusual 2,6-dioxabicyclo[2.2.1]heptane carbocyclic core. The biosynthetic origin for **1** was proposed with the co-isolated **2** as a bio-analogue (Fig. 8). Derived from farnesyl pyrophosphate (FPP) and HDMP[15,16], a series of alkylation and intramolecular cyclization reactions led to the formation of the crucial biosynthetic intermediate, andiconin. Andiconin subsequently participated in many steps of reactions involving oxidation, methoxylation, hemiketal, and Michael addition reactions to furnish the polycyclic scaffold of **1**. In addition, andiconin could also be transformed to **2** via a series of reactions including reduction, dehydration, oxidation, Michael addition, and keto-enol tautomerism.
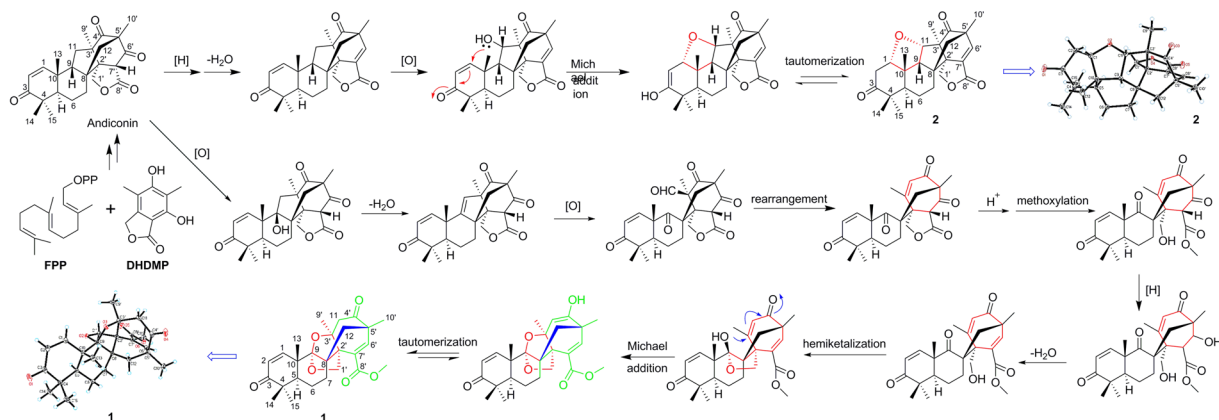
Figure 8. Plausible biosynthetic pathway for compounds **1** and **2**.

Antibiotics	MIC (µg/mL)[a]			$\sum FIC_{1+A}$[c]	$\sum FIC_{2+A}$[c]
	Antibiotic alone (A)	A + Cmpd 1	A + Cmpd 2		
Oxacillin	32	4[b]	16	0.25*	>0.5
Piperacillin	64	4	32	0.375*	>0.5
Chloramphenicol	16	4	16	1.25	≥2.0
Vancomycin	0.5	0.5	0.5	>1.0	>1.0

Table 2. Combination susceptibility test of compounds **1** and **2** with various antibacterial antibiotics against MRSA in Checkerboard assay. [a]The MIC of compounds **1** and **2** alone against MRSA were 32 µg/mL and >100 µg/mL, respectively. The MIC of oxacillin combined with compound **1** against MRSA was 1 µg/mL (oxacillin and **1** were co-dosed at sub-MIC levels, both 1 µg/mL). *Compound **1** was determined to work synergistically with oxacillin and piperacillin, with $\sum FIC$ values of 0.25 and 0.375 However, it did not show any synergistic effect on other antibiotics. [c]$\sum FIC = FIC_{Cmpd} + FIC_{Antibiotic}$; $FIC_{Cmpd} = [MIC_{Cmpd}$ in combination]/ $[MIC_{Cmpd}$ alone]; $FIC_{Antibiotic} = [MIC_{Antibiotic}$ in combination]/$[MIC_{Antibiotic}$ alone]. The combination is considered synergistic when the $\sum FIC$ value is ≤0.5, accumulative or indifferent when the $\sum FIC$ value is >0.5 but <2, and antagonistic when the $\sum FIC$ is ≥2.

Antimicrobial activity. Antibacterial activities against MRSA were observed for **1** with MIC values of 32 µg/ml, whereas compound **2** showed only marginal antimicrobial activity. In addition, compound **1** was found to work synergistically with the β-lactam antibiotics oxacillin and piperacillin with $\sum FIC$ values that were less than 0.5 (Table 2)[14]. To further investigate the antibacterial mechanism of **1**, in silico target confirmation assays[13] were employed to forecast its possible targets. Therefore, **1** was screened against all five PBPs (PBP1, PBP2, PBP2a, PBP3, and PBP4) encoded in the MRSA core genome in silico[8], which were considered to be important or promising targets for staphylococcal β-lactam resistance[9,10,18,19].

Inverse docking identified the possible antibacterial target. The potent antimicrobial activity of compound **1** prompted us to investigate the underlying mechanism. As mentioned above, some complexes of PBPs (PDB ID: 5TRO, 2ZC3, 4CJN, 3PBR and 3HUM) from *S. aureus* were applied in virtual screening. The total-score values (Table 3) predicted that compound **1** was most likely to bind to allosteric site of PBP2a with higher total score value. To further define this speculation, a microscale thermophoresis (MST) method, which has previously been used to investigate protein-protein, small organic molecule-protein and antibody-protein interactions, was employed to assay the binding affinity between the compounds and PBPs[12]. As a result, **1** exhibited the strongest binding with PBP2a (Table 3). The equilibrium dissociation constant (Kd) of **1** was 18.4 ± 1.29 µM (Fig. 9).

Previous research showed the PBP2a as an elongated protein with a transpeptidase domain (residues 327–668) and a nonpenicillin-binding domain (residues 27–326), which includes an N-terminal extension subdomain (residues 27–138). Two major binding sites of PBP2a had been identified: one at the active site, where binding of antibiotic or peptidoglycan is known to take place, and another within the nonpenicillin-binding domain, 60 Å distant from the active site, which was proved to be allosteric site. The further virtual docking revealed that compound **1** possibly bound to the allosteric site of PBP2a, further lead to the opening of the active site, enabling catalysis by PBP2a. This result was consistent with synergistic effect of compound **1** with β-lactam antibiotics. As shown in Fig. 10, key hydrogen-bond interactions were between compound **1** with the residues of Asn104, Asn146 and Lys273. Based on the molecular docking results, importing hydrophilic group substituents placed at the C-6 and C-7 position is a worthy target for further structural modification.

In order to visualize the morphology of the bacteria after treated by the inhibitor, the transmission electron microscopy (TEM) was employed. The evidence of TEM images (Fig. 11) of MRSA treated by compound

PDB ID	Protein name	Compound 1
5TRO	PBP1	2.431
2ZC3	PBP2	1.327
4CJN	PBP2ᵃ	5.163*
3PBR	PBP3	4.129
3HUM	PBP4	2.017

Table 3. Predicted binding free energies of compound **1** with five PBPs of MRSA, which considered to be important or possible media for staphylococcal β-lactam resistance. (Surflx-Dock scores)ᵃ. ᵃDocking score/ interaction potential of compounds with targets (kcal/mol). *The docking scores predicted that PBP2a showed significantly higher binding affinity for **1** than other PBPs.
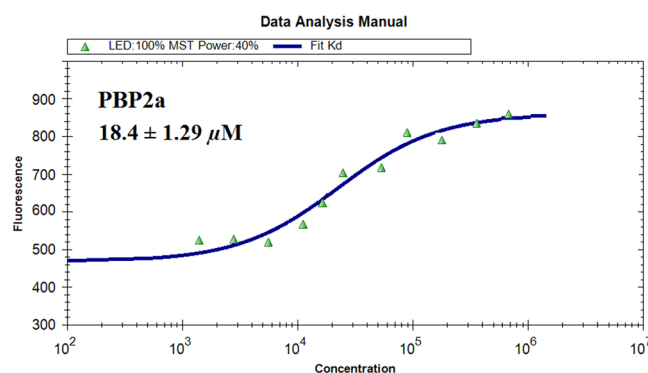
Figure 9. MST confirmed that compound **1** maintained specific binding to MRSA PBP2a. The measurement of the affinity between compound **1** with PBP2a via MST in standard treated capillaries is shown in the resulting binding curve. From the resulting binding curve, Kd $= 18.4 \pm 1.29\,\mu$M for compound **1**.

1 confirmed an obvious change in the ultrastructure of the strains. In the control strains, intact septa were evident, while the strains treated with MIC of compound **1**, appearing irregular membrane damage and disruption (Fig. 11).

In summary, aspermerodione (**1**), a complex polycyclic meroterpenoid containing a rare 2,6-dioxabicyclo[2.2.1] heptane motif and a new biosynthetically related compound, andiconin C (**2**) were isolated and identified from the liquid culture of the endophytic fungus *Aspergillus* sp.TJ23. The structures of both compounds were elucidated by the combined implementation of X-ray crystallography and ECD calculations. A plausible biosynthetic pathway of **1**, involving its bio-metabolite **2**, has been proposed. Our research demonstrates that aspermerodione (**1**) has anti-MRSA activity and based on the observation of TEM, the anti-MRSA activity of **1** might be tightly related to its effect of damaging bacterial cell wall and/or membrane. Moreover, aspermerodione (**1**) acts as a potential inhibitor of PBP2a that works synergistically with the β-lactam antibiotics oxacillin and piperacillin on antibacterial activities against MRSA. Since a promising strategy for combatting MRSA is to extend the lifespan and efficacy of our currently employed drugs using combination therapy, we believe that the disclosed novel chemical structure and bioactivity of **1** may provide a promising precursor for the development of a combination treatment regime against MRSA.

Methods

General. Optical rotations were determined using a Perkin-Elmer 341 polarimeter (PerkinElmer, Waltham, MA, USA). UV and IR spectra were obtained using a Varian Cary 50 (Varian, Salt Lake City, UT, USA) and a Bruker Vertex 70 instrument (Bruker, Karlsruhe, Germany), respectively. ECD spectra were recorded on a JASCO-810 spectropolarimeter. NMR spectroscopic data were recorded on a Bruker AM-400 spectrometer (Bruker, Karlsruhe, Germany), and the ^{1}H and ^{13}C NMR chemical shifts are expressed in δ, referring to the solvent impurity peaks for CDCl$_3$ (δ_H 7.26 and δ_C 77.0). HRESIMS was performed in the positive ion mode on a Thermo Fisher LC-LTQ-Orbitrap XL spectrometer (Thermo Fisher, Palo Alto, CA, USA). Semi-preparative HPLC was conducted on a Dionex HPLC system equipped with an Ultimate 3000 pump (Thermo Fisher, Scientific, Germany), an Ultimate 3000 auto sampler injector, and an Ultimate 3000 diode array detector (DAD) controlled by Chromeleon software (version 6.80), using a reversed-phased C$_{18}$ column (5 μm, 10 × 250 mm, Welch Ultimate XB-C$_{18}$). Column chromatography was performed using silica gel (80–100, 100–200, and 200–300 mesh; Qingdao Marine Chemical Inc., China), ODS (50 μm, Merck, Germany), Sephadex LH-20 (Merck, Germany), and MCI gel (75–150 μm, Merck, Germany). Thin-layer chromatography (TLC) was performed using silica gel 60 F254 (Yantai Chemical Industry Research Institute) and RP-C$_{18}$ F254 plates (Merck, Germany).

Fungus material. The fungus *Aspergillus* sp. TJ23 was isolated from the leaves of the Chinese traditional plant *Hypericum perforatum* (St John' Wort), which was collected from the Shennongjia areas of Hubei Province, China. The sequence data for this strain has been submitted to the DDBJ/EMBL/GenBank with accession
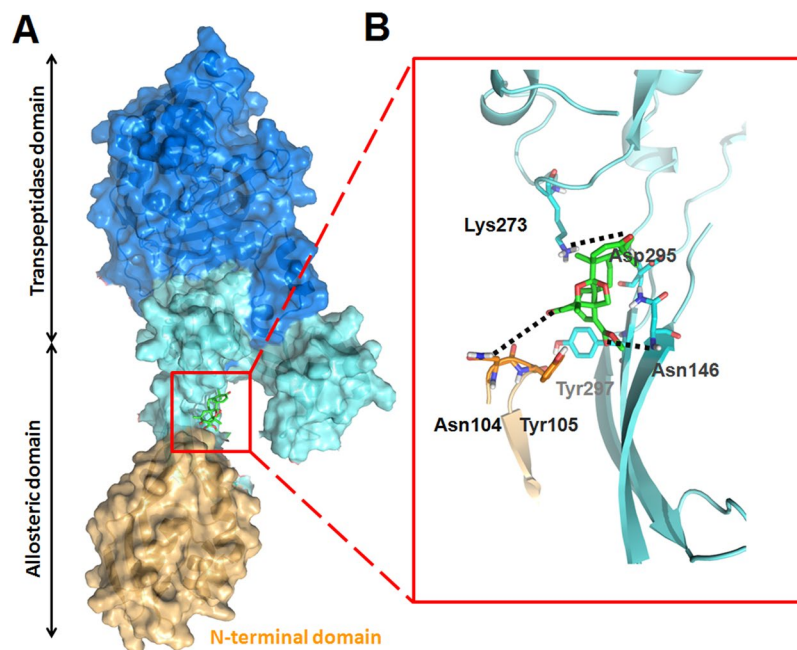
Figure 10. Docking model of PBP2a in complex with compound **1**. (**A**) Ribbon representation of PBP2a showing compound **1** (in green for carbons) bound to the allosteric site. The allosteric domain spans residues 27−326, where the N-terminal domain (residues 27−138) is shown in yellow and the remaining allosteric domain is light blue colored. The transpeptidase domain (residues 327−668) is shown in dark blue. (**C**) Key interactions of compound **1** at the allosteric site. Hydrogen-bond interactions with Asn104, Asn146 and Lys273 are shown as black dashed lines.
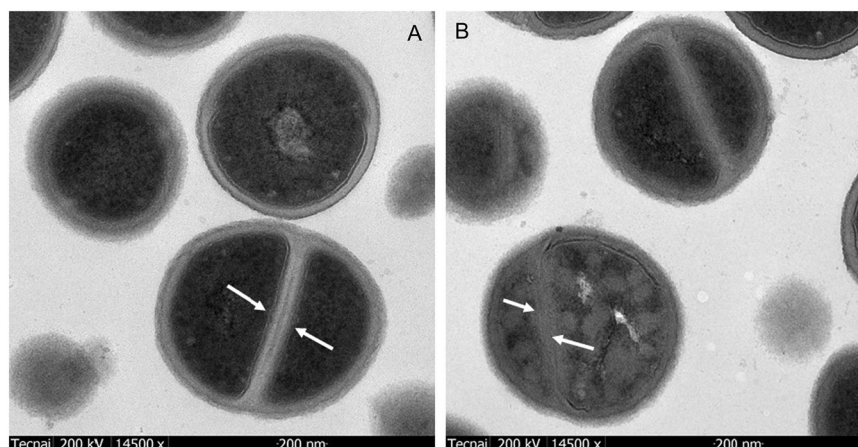
Figure 11. TEM images of MRSA after 30 min of aspermerodione (**1**) treatment. (**A**) Untreated MRSA. The arrows indicate intact septa. (**B**) MRSA treated with the MIC of aspermerodione (32 μg/mL). The arrows indicate irregular membrane damage and disruption.

no. KY346978. The voucher sample was deposited in the culture collection center of Tongji Medical College, Huazhong University of Science and Technology.

Extraction and isolation. Mycelia of the fungus growing on malt extract agar were inoculated in a 250 mL Erlenmeyer flask containing 100 mL of malt extract broth medium [malt extract 2.0% (w/v), glucose 2.0% (w/v) and bacterial peptone 0.1% (w/v)] and cultured statically at room temperature for 30 days. Twenty litres in total of the whole culture broth were then filtered through a filter paper. The mycelia (1.5 kg of wet weight) were extracted with EtOAc (5×2 L). After evaporation of the solvent, a dark brown solid (80.5 g) was obtained, which was extracted with ethyl acetate (5×2 L). The ethyl acetate extract was evaporated under a reduced pressure, leaving a brown viscous residue (6.2 g), which was chromatographed using RP-C_{18} silica gel CC eluted with MeOH–H_2O (20%, 40%, 60%, 80%, and 100%) to afford five fractions (Fr.1–Fr.5). Fr.3 (1.6 g) was further fractionated on a silica gel column eluted with CH_2Cl_2/MeOH (20:1–0:1) to obtain six major fractions (Fr.3.1–Fr.3.6) based on

the TLC analysis. Fr.3.2 (0.6 g) was further separated via semipreparative HPLC (MeOH–H$_2$O, 85%) to afford compounds **1** (20.8 mg; t_R 13.2 min; 2 mL/min) and **2** (14.2 mg; t_R 9.0 min; 2 mL/min), respectively.

Physicochemical data.   *Aspermerodione (***1***)*, colorless crystals (CHCl$_3$–MeOH); mp 214–216 °C; [α] –342 (*c* 0.19, CH$_2$Cl$_2$); UV (CH$_2$Cl$_2$) λ_{max} (log ε) = 230 (4.11), 294 (2.96) nm; IR ν_{max} = 2969, 2940, 1705, 1671, 1622, 1438, 1379, and 1267 cm^{-1}; CD (CH$_2$Cl$_2$) λ_{max} ($\Delta\varepsilon$) 232 (+37.5) and 297 (−42.5) nm; ^{1}H NMR (400 MHz) and ^{13}C NMR (100 MHz) data see Table 1; HRESIMS [M + Na]$^+$ *m/z* 463.2049 and 441.2251 [M + H]$^+$ (calcd for C$_{26}$H$_{32}$O$_6$Na, 463.2097 and C$_{26}$H$_{33}$O$_6$, 441.2277).

    *Andiconin C (***2***)*, colorless crystals (CHCl$_3$–MeOH); mp 279–281 °C; [α] −298.7 (*c* 0.23, MeOH); UV (MeOH) λ_{max} (log ε) = 243 (3.19) and 314 (2.39) nm; IR ν_{max} = 2935, 2876, 1765, 1717, 1664, 1471, 1452 and 1014 cm^{-1}; CD (MeOH) λ_{max} ($\Delta\varepsilon$) 246 (+32.4) and 311 (−35.3) nm; ^{1}H NMR (400 MHz) and ^{13}C NMR (100 MHz) data see Table 1; HRESIMS [M + Na]$^+$ *m/z* 433.1961 and [M + H]$^+$ 411.2146 (calcd for C$_{25}$H$_{32}$O$_6$Na, 433.1991 and C$_{25}$H$_{33}$O$_6$, 411.2171).

Crystal data for 1.   C$_{26}$H$_{32}$O$_6$, M = 440.52, a = 11.96170(10) Å, b = 14.75700(10) Å, c = 12.60300(10) Å, α = 90°, β = 97.1400(10)°, γ = 90°, V = 2207.42(3) Å^3, T = 100(10) K, space group $P2_1$, Z = 2, μ(CuKα) = 0.758 mm^{-1}, 22895 reflections collected, 8337 independent reflections (R_{int} = 0.0207). The final R_1 values were 0.0282 ($I \geq 2\sigma(I)$). The final $wR(F^2)$ values were 0.0726 ($I \geq 2\sigma(I)$). The final R_1 values were 0.0284 (all data). The final $wR(F^2)$ values were 0.0729 (all data). The goodness of fit on F^2 was 1.049. Flack parameter = −0.04(4). Hooft parameter = 0.00(3).

Crystal data for 2.   C$_{25}$H$_{30}$O$_5$, M = 410.49, a = 9.22259(8) Å, b = 14.56007(14) Å, c = 15.09953(13) Å, α = 90°, β = 90°, γ = 90°, V = 2027.59(3) Å^3, T = 100(10) K, space group $P2_12_12_1$, Z = 4, μ(CuKα) = 0.747 mm^{-1}, 14739 reflections collected, 4019 independent reflections (R_{int} = 0.0251). The final R_1 values were 0.0307 ($I \geq 2\sigma(I)$). The final $wR(F^2)$ values were 0.0797 ($I \geq 2\sigma(I)$). The final R_1 values were 0.0310 (all data). The final $wR(F^2)$ values were 0.0799 (all data). The goodness of fit on F^2 was 1.068. Flack parameter = −0.03(5). Hooft parameter = −0.00(5).

    The crystallographic data for compounds **1** and **2** were collected at 100 K on a Rigaku Oxford Diffraction Supernova Dual Source, Cu at Zero equipped with an AtlasS2 CCD using Cu Kα radiation and were deposited in the Cambridge Crystallographic Data Centre. Copies of the data can be obtained free of charge from the Cambridge Crystallographic Data Centre, 12 Union Road, Cambridge CB21EZ, UK (fax: +44-1223-336-033; or e-mail: deposit@ccdc.cam.ac.uk). The structures were solved by direct methods using Olex2 software[20], and the non-hydrogen atoms were located from the trial structure and then refined anisotropically with SHELXL-2014[21] using a full-matrix least squares procedure based on F^2. The weighted R factor, wR and goodness-of-fit S values were obtained based on F^2. The hydrogen atom positions were fixed geometrically at the calculated distances and allowed to ride on their parent atoms.

ECD calculation details.   The conformations of **1** and **2** generated by BALLOON[22,23] were subjected to semiempirical PM3 quantum mechanical geometry optimizations using the Gaussian 09 program[24]. Duplicate conformations were identified and removed when the root-mean-square (RMS) distance was less than 0.5 Å for any two geometrically optimized conformations. The remaining conformations were further optimized at the B3LYP/6-31 G(d) level in MeOH with the IEFPCM solvation model using Gaussian 09, and the duplicate conformations emerging after these calculations were removed according to the same RMS criteria above. The harmonic vibrational frequencies were calculated to confirm the stability of the final conformers. The electronic circular dichroism (ECD) spectrum was calculated for each conformer using the TDDFT methodology at the LC-wPBE/6-311++G(d,p)//B3LYP/6-31 G(d) level with MeOH as the solvent via the IEFPCM solvation model implemented in the Gaussian 09 program. The ECD spectrum for each conformer was simulated using a Gaussian function with a bandwidth, σ, of 0.4 eV. The spectra were combined after Boltzmann weighting according to their population contributions, and a UV correction was applied[25].

Biological Activities Evaluation
Strains, media, and antibiotics.   The tested MRSA strain was obtained from the ATCC: MRSA (ATCC 43300). The reference compounds for the tests were recommended by the National Committee for Clinical Laboratory Standards[26]. Oxacillin (Sigma, cat # 1481000); Piperacillin (Sigma, cat # 1541500); Chloramphenicol (Sigma, cat # 1107300); Vancomycin (Sigma, cat # 861987). Meropenem (Sigma, cat # M2574). Investigated compounds **1** and **2** were ≥95% pure (HPLC, wavelength = 210 nm). All compounds were dissolved in DMSO as 20 mg/mL stock solutions.

Determination of the minimum inhibitory concentrations (MIC).   Determination of the MICs were conducted according to our previously reported broth microdilution method[12,13]. In brief, the inoculum was standardized to approximately 5×10^5 CFU/mL. The plates were incubated at 37 °C for 16 h, and the MIC values were recorded as the lowest concentration of antibiotic at which no visible bacterial growths were observed. Each experiment was performed three times.

Combination susceptibility test against MRSA.   Determination of the combination susceptibility was conducted according to our previously reported broth microdilution checkerboard assay[12,13]. MHB was inoculated with MRSA (5×10^5 CFU/mL), and 100 μL was distributed into each well of a 96-well plate except in well 1 A. Inoculated MHB (200 μL) containing test compound (at 2 × MIC) were added to well 1 A, and 100 μL of the same sample was placed in each of well for 2A-12A. Column A wells were mixed 6 to 8 times, and then 100 μL was withdrawn and transferred to column B. Column B wells were mixed 6 to 8 times, followed by a 100 μL transfer

to column C. This procedure was repeated to serially dilute the rest of the columns of the plate up to column G (column H was not mixed to allow the MIC of the antibiotic alone to be determined). Inoculated media (100 μL) containing the antibiotic at two times, the MIC was placed in wells A1-H1 (row 1) and serially diluted in the same manner as row 11. The plates were incubated for 16 h at 37 °C. The MIC values of both compounds and the antibiotic in the combination were recorded as well as the MIC values of the compound alone (row 12) and antibiotic alone (column H). The $\sum$FIC values were calculated as follows: $\sum FIC = FIC_{Compd} + FIC_{Antibiotic}$, where FIC_{Compd} is the MIC of the compound in the combination/MIC of the compound alone, and $FIC_{Antibiotic}$ is the MIC of the antibiotic in the combination/MIC of the antibiotic. The combination is considered synergistic when the $\sum$FIC value is ≤ 0.5, accumulative or indifferent when the $\sum$FIC value is >0.5 but <2, and antagonistic when the $\sum$FIC is ≥ 2[27].

Molecular docking and virtual screening.
The compounds were saved as mol2 files and used as an input for docking. The docking was performed using the Surflx-Dock module of the Sybyl softare[28,29]. Ligand binding pocket residues were selected using graphical tools in the Sybyl software to create the boundaries of the docking search. All of the hydrogen atoms were added to define the correct ionization and tautomeric states, and the carboxylate, phosphonate and sulphonate groups were considered in their charged form. In the docking calculation, the default FlexX scoring function was used for exhaustive searching, solid body optimizing and interaction scoring[28,29]. The pose with the lowest-energy and the most favorable score was remained.

Protein expression and purification.
Wild-type PBP2a (residues 23-668) and four other PBPs (PBPs 1–4) were cloned into a pET28a vector (EMD Biosciences, Novagen, United States) from the *mec*A sequence of *Staphylococcus aureus* ATCC 43300. After confirmation by DNA sequencing, the recombinant plasmid was transferred into *Escherichia coli* strain, BL21 (DE3). The transformed cells were grown in LB medium at 37 °C to an OD_{600} (0.8–1.0) and induced with 0.4 mM of isopropyl-D-thiogalactopyranoside (IPTG) at 293 K for 16 h. After they were harvested via centrifugation, the cells were re-suspended on ice in a lysis buffer containing 20 mM Tris (pH 7.5), 200 mM NaCl, and 10 mM imidazole, followed by disruption on a French press. Cell debris was removed via centrifugation at 21,000 rpm for 30 min. The protein was bound to Ni-agarose affinity resin, washed with a buffer containing 20 mM Tris (pH 7.5), 200 mM NaCl, and 10 mM imidazole, and eluted with a buffer containing 20 mM Tris (pH 7.5), 250 mM NaCl, and 150 mM imidazole. Fractions containing PBP2a were pooled and further purified on Sephacryl S-200 size-exclusion resin in 2 mM of Tris (pH 7.5) and 200 mM of NaCl.

Microscale thermophoresis.
Recombinant PBP2a and four other PBPs (PBPs 1–4) were labelled with the Monolith NT™ Protein Labelling Kit, RED (Cat # L001), according to the supplied labelling protocol. Labelled PBPs was used at a concentration of 50 nM. Samples were diluted in a 20 mM HEPES (pH 7.4) and 0.05 (v/v)% Tween-20. We used 5 mM of compounds **1** and **2** as the highest concentration for the serial dilution. Oxacillin and Meropenem were used as positive controls. After 10 min of incubation at room temperature, the samples were loaded into Monolith™ standard-treated capillaries, and the thermophoresis was measured at 25 °C after 30 min of incubation on a Monolith NT.115 instrument (NanoTemper Technologies, München, Germany). The laser power was set to 20% or 40% using 30 seconds on-time. The LED power was set to 100%. The dissociation constant, Kd, values were fitted by using the NTAnalysis software (NanoTemper Technologies, München, Germany)[30].

Transmission electron microscopy (TEM).
Mid-logarithmic grown MRSA was collected by centrifugation at 10,000 g for 10 min, and fixed with modified Karnovsky's fixative. Then the specimens were examined using an energy-filtering transmission electron microscope (Tecnai G2 20 TWIN, FEI, Oregon, USA) operated at 200 kV accelerating voltage.

Statistical analysis.
The Graph Pad Prism 5.0 software was employed to analyze the statistical data, with the outcome expressed as the means $\pm$ SD. Values were analysed using SPSS version 12.0 software by one-way analysis of variance (ANOVA), and a $p < 0.05$ was considered statistically significant.

References

1. Diekema, D. J. *et al.* Survey of infections due to Staphylococcus species: frequency of occurrence and antimicrobial susceptibility of isolates collected in the United States, Canada, Latin America, Europe, and the Western Pacific Region for the SENTRY Antimicrobial Surveillance Program, 1997–1999. *Clin. Infec. Dis.* **32**, S114–S132 (2001).
2. Boucher, H. W. *et al.* Bad bugs, no drugs: no ESKAPE! An update from the Infectious Diseases Society of America. *Clin. Infec. Dis.* **48**, 1–12 (2009).
3. Klevens, R. M. *et al.* Invasive methicillin-resistant Staphylococcus aureus infections in the United States. *J. Am. Med. Assoc.* **298**, 1763–1771 (2007).
4. Fuda, C. C., Fisher, J. F. & Mobashery, S. Beta-lactam resistance in Staphylococcus aureus: the adaptive resistance of a plastic genome. *Cell. Mol. Life Sci.* **62**, 2617–2633 (2005).
5. Malouin, F. & Bryan, L. E. Modification of penicillin-binding proteins as mechanisms of beta-lactam resistance. *Antimicrob. Agents Chemother.* **30**, 1–5 (1986).
6. Fuda, C., Suvorov, M., Vakulenko, S. B. & Mobashery, S. The basis for resistance to β-lactam antibiotics by penicillin-binding protein 2a of methicillin-resistant Staphylococcus aureus. *J. Biol. Chem.* **279**, 40802–40806 (2004).
7. Fuda, C. *et al.* Activation for catalysis of penicillin-binding protein 2a from methicillin-resistant Staphylococcus aureus by bacterial cell wall. *J. Am. Chem. Soc.* **127**, 2056–2057 (2005).
8. Otero, L. H. *et al.* How allosteric control of Staphylococcus aureus penicillin binding protein 2a enables methicillin resistance and physiological function. *Proc. Natl. Acad. Sci. USA* **110**, 16808–16813 (2013).
9. Bush, K. Antibiotics: Synergistic MRSA combinations. *Nat. Chem. Biol.* **11**, 832–833 (2015).
10. Gonzales, P. R. *et al.* Synergistic, collaterally sensitive beta-lactam combinations suppress resistance in MRSA. *Nat. Chem. Biol.* **11**, 855–861 (2015).

11. Qiao, Y. *et al.* Diterpenoids of the cassane type from *caesalpinia decapetala*. *J. Nat. Prod.* **79**, 3134–3142 (2016).
12. He, Y. *et al.* Fungal naphtho-γ-pyrones: potent antibiotics for drug-resistant microbial pathogens. *Sci. Rep.* **6**, 24291 (2016).
13. He, Y. *et al.* Spiroaspertrione A, a bridged spirocyclic meroterpenoid, as a potent potentiator of oxacillin against methicillin-resistant Staphylococcus aureus from Aspergillus sp. TJ23. *J. Org. Chem.* **82**, 3125–3131 (2017).
14. Grothe, E., Moo-Young, M. & Chisti, Y. Fermentation optimization for the production of poly(β-hydroxybutyric acid) microbial thermoplastic. *Enzyme. Microb. Tech.* **25**, 132–141 (1999).
15. Matsuda, Y. & Abe, I. Biosynthesis of fungal meroterpenoids. *Nat. Prod. Rep.* **33**, 26–53 (2016).
16. Matsuda, Y., Wakimoto, T., Mori, T., Awakawa, T. & Abe, I. Complete biosynthetic pathway of anditomin: Nature's sophisticated synthetic route to a complex fungal meroterpenoid. *J. Am. Chem. Soc.* **136**, 15326–15336 (2014).
17. Flack, H. D. & Bernardinelli, G. *Acta Crystallogr.* **55**, 908–915 (1999).
18. Chan, L. C. *et al.* PBP4 mediates high-level resistance to new-generation cephalosporins in Staphylococcus aureus. *Antimicrob. Agents Chemother.* **60**, 3934 (2016).
19. Berti, A. D. *et al.* Penicillin binding protein 1 is Important in the compensatory response of Staphylococcus aureus to daptomycin-Induced membrane damage and is a potential target for β-Lactam-daptomycin synergy. *Antimicrob. Agents Chemother.* **60**, 451–458 (2016).
20. Dolomanov, O. V., Bourhis, L. J., Gildea, R. J., Howard, J. A. K. & Puschmann, H. OLEX2: a complete structure solution, refinement and analysis program. *J. Appl. Crystallogr.* **42**, 339–341 (2009).
21. Sheldrick, G. M. A short history of SHELX. *Acta crystallogr.* **64**, 112–122 (2008).
22. Vainio, M. J. & Johnson, M. S. Generating conformer ensembles using a multiobjective genetic algorithm. *J. Chem. Inf. Model.* **47**, 2462–2474 (2007).
23. Puranen, J. S., Vainio, M. J. & Johnson, M. S. Accurate conformation-dependent molecular electrostatic potentials for high-throughput in silico drug discovery. *J. Comput. Chem.* **31**, 1722–1732 (2010).
24. Frisch, M. J. *et al. Gaussian09, Revision C.01*, Gaussian Inc.: Wallingford, CT, USA, 2010.
25. Zhu, H. J. *Organic stereochemistry: experimental and computational methods*. Ch. 4, 87–105, John Wiley and Sons Ltd (2015).
26. Barry, A. L. *et al.* Methods for determining bactericidal activity of antimicrobial agents: approved guideline. *Natl. Comm. Clin. Lab. Stand.* **19**, 8–12 (1999).
27. Harris, T. L., Worthington, R. J. & Melander, C. Potent small molecule suppression of oxacillin resistance in MRSA. *Angew. Chem. Int. Ed.* **51**, 11254–11257 (2012).
28. Hu, L. *et al.* (±)-Japonones A and B, two pairs of new enantiomers with anti-KSHV activities from Hypericum japonicum. *Sci. Rep.* **6**, 27588 (2016).
29. Hu, Z. *et al.* Phomopsterones A and B, two functionalized ergostane-type steroids from the endophytic fungus Phomopsis sp. TJ507A. *Org. Lett.* **19**, 258–261 (2017).
30. Li, Z. & Scheraga, H. A. Monte carlo-minimization approach to the multiple-minima problem in protein folding. *Proc. Natl. Acad. Sci. USA* **84**, 6611–6615 (1987).

Acknowledgements

Author Contributions

Y.Q., X.Z., Y.H. and W.S. contributed equally to this work. They conducted the main experiments, data analyzes, and wrote the manuscript; W.F., Z.H. and Q.X. assisted the isolated experiments; J.L. performed the ECD calculations; H.Z., J.Z. and Z.L. analyzed the spectroscopic data; Y.Z., Y.X. and J.W. designed the experiments and commented the manuscript. All authors reviewed the manuscript.

Additional Information

Supplementary information accompanies this paper at https://doi.org/10.1038/s41598-018-23817-1.

Competing Interests: The authors declare no competing interests.

Publisher's note: Springer Nature remains neutral with regard to jurisdictional claims in published maps and institutional affiliations.